Sampling Field Heterogeneity at the Heme of *c*-Type Cytochromes by Spectral Hole Burning Spectroscopy and Electrostatic Calculations

Monique Laberge,* Martin Köhler,# Jane M. Vanderkooi,§ and Josef Friedrich#

*Institute of Biophysics, Semmelweis University of Medicine, H-1088 Budapest, Hungary; #Technische Universität München, Lehrstuhl für Physik Weihenstephan, D-85350 Freising, Germany; and §Johnson Research Foundation, Department of Biochemistry and Biophysics, School of Medicine, University of Pennsylvania, Philadelphia, Pennsylvania 19104 USA

ABSTRACT We report on a comparative investigation of the heme pocket fields of two Zn-substituted *c*-type cytochromes—namely yeast and horse heart cytochromes *c*—using a combination of hole burning Stark spectroscopy and electrostatic calculations. The spectral hole burning experiments are consistent with different pocket fields experienced at the hemes of the respective cytochromes. In the case of horse heart Zn-cytochrome *c*, two distinguishable electronic origins with different electrostatic properties are observed. The yeast species, on the other hand, displays a single electronic origin. Electrostatic calculations and graphics modeling using the linearized finite-difference Poisson-Boltzmann equation performed at selected time intervals on nanosecond-molecular dynamics trajectories show that the hemes of the respective cytochromes sample different potentials as they explore conformational space. The electrostatic potentials generated by the protein matrix at the heme show different patterns in both cytochromes, and we suggest that the cytochromes differ by the number of "electrostatic substates" that they can sample, thus accounting for the different spectral populations observed in the two cytochromes.

INTRODUCTION

Heme proteins have a porphyrin active group that is central to their specific function, and among the questions generating significant interest is the description of the interaction between prosthetic groups and apoprotein, as mediated by the field generated by the protein matrix (Köhler et al., 1998; Laberge, 1998). Cytochrome *c* is a good candidate for such studies, because the heme is well characterized spectroscopically (Gouterman, 1978; Loew, 1983), and high-resolution x-ray and NMR structures are also available for several cytochromes. The study of protein electrostatic field effects is most relevant to the question of the structural heterogeneity of proteins, which is of considerable interest in biophysics (Campbell et al., 1987; Frauenfelder and Wolynes, 1994). It is, of course, directly related to the possible conformations that a protein can adopt to perform its biological function. That various molecular conformations can play different roles in chemical processes and that conformational rearrangements can lead to a variety of stable and functional species is now well known. The fundamental role of electrostatics in macromolecular function is also well established (Harvey, 1989; Northrup et al., 1990; Sharp and Honig, 1990; Warshel and Aqvist, 1991) and supported by substantial recent studies pointing to the functional significance of the local electrostatic fields generated by a protein as it samples functional space (Furenlid et al., 1990; Lamotte-Brasseur et al., 1990; Avbelj and Moult, 1995; Paulsen and Ornstein, 1995; Sitnitsky, 1995).

In the context of heme proteins, electrostatic interactions have been shown to be of significant importance in facilitating the association of reaction complexes (Gunner and Honig, 1991; Langen et al., 1992; Zhou, 1993; Zhou and Kostic, 1993), and recent site-directed mutagenesis work has firmly established that a combination of solvation effects and H-bonding interactions is involved in the control of the charge distribution at the heme and of its molecular geometry (Davies et al., 1993; Hildebrandt et al., 1993). A theoretical study carried out on a number of cytochrome *c* conformers generated by molecular dynamic simulations suggested that conformations of the protein different from that of the time-averaged structure may prove crucial for protein function (Wendoloski and Matthew, 1989). In their comprehensive study of the influence of the protein matrix on the heme geometry of several heme proteins, Shelnutt et al. have also convincingly shown that protein-induced differences in the nonplanarity of the heme could account for the specificity of their respective biological functions (Hobbs and Shelnutt, 1995).

We have recently started investigating local electric fields in the heme pocket of derivatives of *c*-type cytochromes by hole burning Stark effect spectroscopy, and we were able to observe how they are influenced by specific heme pocket residues and the occurrence of pocket charge redistribution effects (Köhler et al., 1996, 1997).

HH*c* is known to exhibit a specific type of conformational heterogeneity, undetected in the x-ray structure but resolved by NMR, at pH 7 in the region surrounding the heme (Burns and La Mar, 1981). Although this cytochrome has been shown to exist in different conformations at acidic or alkaline pH (Dickerson and Timkovich, 1975), conven-

Received for publication 29 August 1998 and in final form 26 August 1999.

Address reprint requests to Dr. Josef Friedrich, Technische Universität München, Lehrstuhl für Physik Weihenstephan, Vöttinger Str. 40, D-85350 Freising, Germany. Tel.: 49-8161-71-3294; Fax: 49-8161-71-4517; E-mail: j.friedrich@lrz.tu-muenchen.de.

0006-3495/99/12/3293/12 $2.00

tional spectroscopy results had previously failed to distinguish between different conformers at physiological pH.

The present work reports on spectral hole burning (SHB)-Stark effect experiments performed on two *c*-type cytochromes, namely from horse heart (HHZn*c*) and yeast (YZn*c*), and on the generation of different protein conformations from nanosecond-molecular dynamics trajectories. The distinct spectral populations—indicative of field heterogeneity at the heme–are then correlated with the variations in electrostatic potential calculated at the hemes as the proteins sample conformational space. With this approach, we wish to address the question of the dynamic aspect of protein structure and investigate whether, in its fluctuations, a protein can adopt different electrostatic conformations capable of affecting the field experienced at the heme. The results allow us to comment on different patterns of charge reorganization in the heme pockets of HHZn*c* and YZn*c*, consistent with their different SHB profiles in external electric fields.

MATERIALS AND METHODS

Sample preparation

HHZn*c* and YZn*c* were prepared as fully described elsewhere (Vanderkooi et al., 1976). Lyophilized protein was dissolved in 10 mM phosphate buffer (~10 mg/ml, pH 7), and glycerol was used in a 1:2 volume ratio to achieve good optical quality at cryogenic temperatures. At room temperature, the $B_{(0,0)}$ transition occurs at 23,641 cm^{-1}, and $Q_{(0,0)}$ and $Q_{(0,1)}$ are observed at 17,094 and 18,215 cm^{-1}, respectively. Holes were burned in the $Q_{(0,0)}$ region.

Spectral hole burning-Stark effect spectroscopy

The behavior of spectral holes in an external electric field contains information about the dipole moment difference between the ground and excited states of the chromophore (Köhler et al., 1998). A dipole moment difference can arise as follows: either the chromophore has no inversion center ("permanent dipole moment difference"), or it has one with the inversion symmetry destroyed by the local electric field generated by the matrix ("induced dipole moment difference") (Gottfried et al., 1991; Gafert et al., 1995; Köhler et al., 1996).

The chromophore used as the optical probe in this work is the Zn-substituted heme of the cytochromes. Stark experiments in a glass matrix showed that it is almost centrosymmetrical (Köhler et al., 1996). Therefore, all observed dipole moments must be induced by the protein matrix, either through protonation of the propionics, through a change in the geometry, or through electronic polarization of the chromophore by the pocket field.

Through the interaction of the dipole moments with the electric field **E** acting on the chromophore, the spectral lines experience a shift $\Delta\nu$, the so-called Stark shift:

$$\Delta\nu = -1/hc[\mathbf{E}\Delta\boldsymbol{\mu}_{\mathrm{mol}} + \tfrac{1}{2}\mathbf{E}\Delta\hat{\alpha}\mathbf{E}] \tag{1}$$

$\Delta\boldsymbol{\mu}_{\mathrm{mol}}$ is the difference between the intrinsic dipole moments of the states involved. $\Delta\hat{\alpha}$ is the difference between the respective molecular polarizability tensors. Because our probe molecule is centrosymmetrical, there is no dipole moment, and hence the first term is zero. **E** is the sum of the so-called pocket field $\mathbf{E}_{\mathrm{pocket}}$ generated by the protein environment at the probe and the external field $\mathbf{E}_{\mathrm{St}}$, which we will call the Stark field. However, $\mathbf{E}_{\mathrm{St}}$ is modified by a factor f which accounts for the shielding through the dielectric medium with the permittivity ϵ:

$$\mathbf{E} = \mathbf{E}_{\mathrm{pocket}} + f\mathbf{E}_{\mathrm{St}} \tag{2}$$

$$f = 3/[2\epsilon + 1] \tag{3}$$

Accordingly, the Stark shift of a centrosymmetrical probe induced by the field **E** consists of three different terms:

$$\Delta\nu = -1/hc[f\mathbf{E}_{\mathrm{pocket}}\Delta\hat{\alpha}\mathbf{E}_{\mathrm{St}} + \tfrac{1}{2}f^2\mathbf{E}_{\mathrm{St}}\Delta\hat{\alpha}\mathbf{E}_{\mathrm{St}} + \tfrac{1}{2}\mathbf{E}_{\mathrm{pocket}}\Delta\hat{\alpha}\mathbf{E}_{\mathrm{pocket}}] \tag{4}$$

The last term is the electrostatic solvent shift, which we will not consider here. The second term is the usual quadratic Stark shift, which is negligibly small because $\mathbf{E}_{\mathrm{St}}$ is several orders of magnitude smaller than $\mathbf{E}_{\mathrm{pocket}}$ (Schmidt and Reich, 1972; Gottfried et al., 1991; Grewer and Lösche, 1991; Kohler et al., 1994). The interesting term is the first one, which we call the pseudolinear Stark shift, to account for the fact that this term is linear in $\mathbf{E}_{\mathrm{St}}$ but scales with $\Delta\hat{\alpha}$ (Köhler et al., 1998).

The lineshape of the hole is a convolution of the hole in the population density $N(\nu_{\mathrm{B}} - \nu' - \Delta\nu_{\mathrm{B}})$ with the absorption lineshape $a(\nu - \nu' - \Delta\nu)$, where $\Delta\nu_{\mathrm{B}}$ and $\Delta\nu$ are the Stark shifts during burning and reading, respectively. These shifts can be different, depending on the fields applied. The lineshapes are very well represented by Lorentzians. Note that the Stark shift depends on the orientation of the dipole moment difference vector $\mathbf{E}_{\mathrm{pocket}} \cdot \Delta\hat{\alpha}$ with respect to the external field (Eq. 4). If we consider solutions of protein molecules as a homogeneous, isotropic matrix for the embedded optical center, this orientation is subject to a distribution; hence the shift experiences a dispersion that contributes to the broadening of the hole in an external electric field, even if $\mathbf{E}_{\mathrm{pocket}}$ does not have any random component. We stress that the orientational angle between $\mathbf{E}_{\mathrm{st}}$ and $\mathbf{E}_{\mathrm{pocket}}$ (or the induced dipole moment difference vector) can be experimentally controlled to some extent by burning the holes with polarized light. The relevant orientational quantity is the angle φ between the transition dipole moment and the difference vector of the permanent dipole moments, which, in turn, determines the angle between the difference vector and $\mathbf{E}_{\mathrm{St}}$ (Maier, 1986; Schätz and Maier, 1987). Below we discuss how the characteristic features of the hole burning Stark spectra depend on the angle φ.

In proteins which, despite their high degree of organization, also exhibit disorder, two types of matrix-induced dipole moment differences can be distinguished: the first type is characterized by a well-defined magnitude and direction in the frame of the chromophore ("fixed dipole moment difference"), because the inducing field is ordered, whereas the second is a statistically induced dipole moment difference due to structural disorder. The occurrence of a fixed dipole moment difference can be inferred from the shape of the hole after applying an external electric field: if there is only a statistically induced dipole moment, the hole will only broaden in the field. If there is a fixed dipole moment difference, the hole will also split in the electric field. From the width of the splitting, the absolute value of the total (intrinsic plus induced) dipole moment difference can then be calculated, provided the dielectric permittivity is known.

As mentioned above, a Stark effect hole burning experiment yields information not only about the absolute value of the dipole moment difference of the chromophore, but also about its direction with respect to the transition dipole moment. To get direction-dependent information, the following experimental geometry was selected: the external electric field was applied perpendicular to the k-vector of the laser light. Two holes were burned: one with laser polarization parallel to the external electric field ($\mathbf{E}_{\mathrm{L}} \parallel \mathbf{E}_{\mathrm{St}}$) and one with perpendicular polarization ($\mathbf{E}_{\mathrm{L}} \perp \mathbf{E}_{\mathrm{St}}$). $\mathbf{E}_{\mathrm{L}}$ and $\mathbf{E}_{\mathrm{St}}$ represent the laser field and the Stark field, respectively. If the angle φ is smaller than 55°, the hole is expected to split under parallel polarization. If it is larger than 55°, the hole splits under perpendicular polarization.

Holes were burned by irradiating the sample within the frequency range of the inhomogeneous Q(0,0)-absorption band, using a ring dye laser (Coherent 899-21) pumped by a single-mode argon ion laser (Coherent Innova Sabre). Some of the molecules absorbing at the frequency of the laser undergo a photochemical or photophysical transition, causing a shift

in their absorption frequency. Thus, at the frequency of the irradiated light, the number of absorbing molecules is decreased. In our system, the width of a spectral hole is on the order of 1 GHz (at 1.7 K). The lifetimes of our holes were long enough to ensure good measurement of the hole profiles at different electric field strengths. When the hole profiles were measured, the intensity of the laser was decreased by a factor of 100-1000 to avoid additional burning. The laser frequency was scanned over the range of the hole, and the frequency-dependent optical density of the sample was recorded. After a hole spectrum was taken at zero field, the electric field was varied in increments up to 22 kV/cm, and hole spectra were recorded at every field step.

COMPUTATIONAL METHODS

Energy minimization

The starting structures were obtained from the Protein Data Bank (Bernstein et al., 1977): pdb1hrc.ent for horse heart cytochrome *c* (Bushnell et al., 1990) and pdb1ycc.ent for yeast cytochrome *c* (Louie and Brayer, 1990), both of which contain waters identified in the x-ray structure that were retained in the minimization. The energy of the structures was minimized using the Discover-3 module of the InsightII software package (MSI, San Diego, CA) on a Silicon Graphics IRIS Indigo workstation, using the ESFF force field modified for a Zn-containing heme group per standard procedure (Laberge et al., 1996; cf. Fig. 1 and Table 1 for heme atom nomenclature and partial charges). The charge distribution of the Glu, Asp, Arg, and Lys residues was set to be representative of pH 7.0. The heme propionates were considered deprotonated and accordingly charged (Wright et al., 1997). Missing hydrogens were added subject to van der Waals constraints. A nonbonded cutoff distance of 15 Å was used for both van der Waals and electrostatic interactions, together with a switching function of 1.5 Å to minimize cutoff discontinuities. To remove artifacts introduced by the addition of explicit hydrogens, the structures were first subjected to a steepest descent minimization to achieve a maximum derivative of less than 5 kcal mol^{-1}, followed by a conjugate gradient using a Newton-Raphson algorithm for which a residual maximum gradient of 0.1 kcal mol^{-1} was set as the convergence criterion. The proteins were then solvated in a 12-Å layer of solvent consisting of 2700 water molecules, and the ensemble was reminimized as before.

Molecular dynamics

For the molecular dynamics (MDS), the minimized structures of both solvated cytochromes were used as starting structures. The simulations were also performed with the ESFF force field and carried out at a constant temperature of

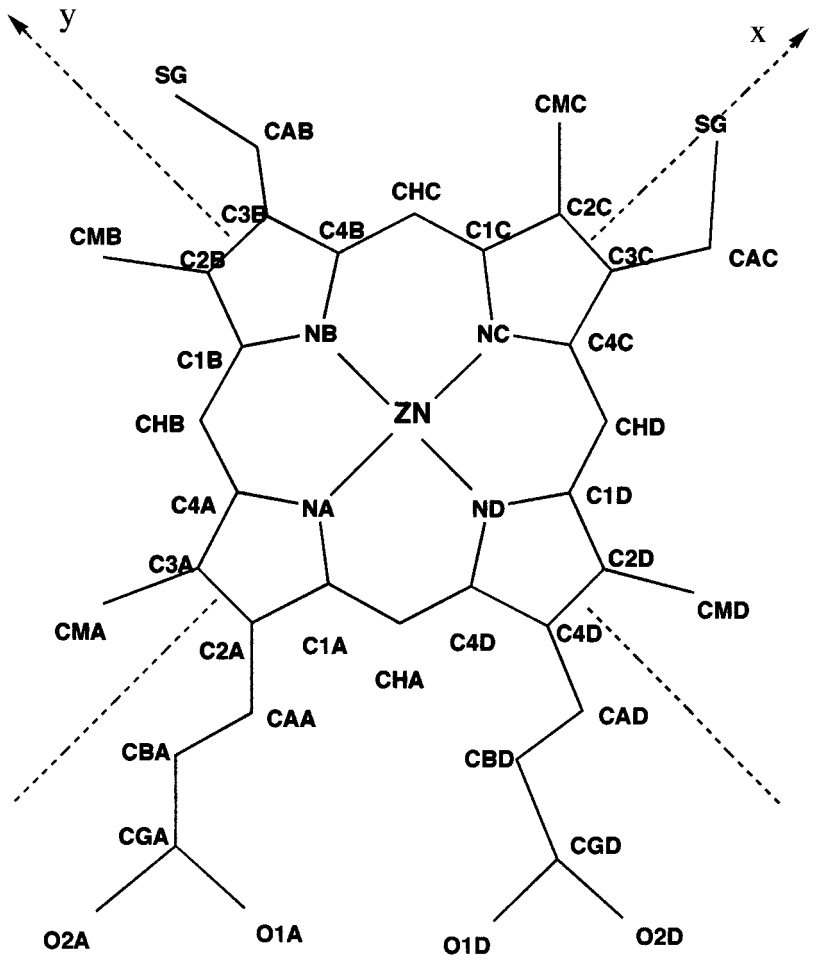

FIGURE 1 Brookhaven Protein Data Bank standard atom nomenclature for a metal-substituted protoheme. The *x* and *y* axes represent the two possible orientations of the transition dipole moment for the possible a_{1u}, $a_{2u} \rightarrow e_g$ transitions (Adar, 1978).

TABLE 1 ESFF atom types and partial charges for Zn-substituted protoheme in horse heart and yeast cytochromes *c*

Atom Type*	PDB Nomenclature	Description	Charge/e
cp	C1A, C4A, C1B, C4B,	Pyrrole carbon	0.145
	C1C, C4C, C1D, C4D	Pyrrole carbon	0.145
cp	CHC, CHD, CHA, CHB	Porphyrin methine carbon	0.103
cp	C2A, C3D	Pyrrole methine carbon +prop-group	−0.028
cp	C3A, C2B, C2C, C2D	Pyrrole c with CH_3 group	−0.046
cp	C3B, C3C	Pyrrole c with vinyl group	0.028
c	CAA, CAD	Propionate carbon	0.011
c	CBA, CBD	Propionate carbon	−0.170
np	NE2	His nitrogen coordinated to Zn	−0.334
np	NA	Pyrrole nitrogen	−0.468
np	NB	Pyrrole nitrogen	−0.468
np	NC	Pyrrole nitrogen	−0.468
np	ND	Pyrrole nitrogen	−0.468
Zn026	ZN	Zn(II)	1.159
c	CMA, CMB, CMC, CMD	CH_3 carbons	−0.032
c	CAC, CAB	Vinyl carbon	−0.043
c	CBB, CBC	Vinyl carbon	−0.047
o′	O1A, O1D	Propionate oxygens	−0.589
oa	O2A, O2D	Propionate oxygens	−0.523
c-	CGA, CGD	Carbon coordinated to propionate oxygen	0.604
h	HHC, HHD, HHB, HHA	Methine hydrogen	0.107
h	HBA1, HBA2	Propionate hydrogen	0.098
h	HAA1, HAA2	Propionate hydrogen	0.063
h	HMA1,2,3; HMB1,2,3;	Methyl hydrogen	0.050
h	HMC1,2,3; HMD1,2,3	Methyl hydrogen	0.050
h	HAB, HAC	Vinyl hydrogen	0.105
h	HBB1,2,3; HBC1,2,3	Vinyl hydrogen	0.044
s	SG	Thioether linkage sulfur	−0.222

*cp, sp^2 aromatic carbon (partial double bands); c, sp^3 carbon; np, sp^2 aromatic nitrogen (partial double bands); Zn026, 6-coordinated Zn; o′, c═o oxygen, oa, sp^3 oxygen, c-, carbon in charged carboxylate; h, generic hydrogen; s, se^3 sulfur.

300 K, using a leapfrog algorithm with a time step of 1 fs. The system was brought to 300 K over 20 ps and equilibrated over 5000 steps. Nonbond interactions were accounted for using the cell-multipole method (Schmidt and Lee, 1991; Ding et al., 1992), which is more rigorous than the application of cut-offs because it calculates both the near-field interactions due to immediate neighbor atoms and the far-field interactions due to the ensemble of atoms. Because these interactions scale as N^2, they are difficult to compute for large solvated ensembles. The cell multipole method represents the potential associated with each basic cell as a general potential located in the center of the cell, which it then expands into an infinite series of multipole moments. Summing the far-field contributions yields the far-field potentials, which can then be expanded as a Taylor series (Ding et al., 1992). The cell multipole approach is thus an "order N" method and results in significant CPU savings, but not at the expense of accuracy. Six independent 1-ns trajectories were recorded for each solvated cytochrome, and the last 500 ps was used for the electrostatic calculations.

Sampling of heme electrostatic potentials in conformational space

To select protein trajectory frames representative of significantly different protein topographies for calculation of the heme potentials, we used an algorithm performing a clustering conformational search that compared each frame or conformation in a trajectory with all others and classified them as pairs of topographical substates, based on the rms comparison of superposed backbone atoms, i.e., C, CA, N, O:

$$\text{rms} = [\Sigma\{(x_i - x_i')^2 + (y_i - y_i')^2 + (z_i - z_i')^2\}/N]^{1/2} \quad (5)$$

The superposition aligned N atoms of one protein trajectory frame with N atoms of another frame, with x_i, y_i, and z_i representing the spatial coordinates of the protein captured in one frame and x_i', y_i', and z_i' the coordinates of the superposed molecule. All conformations in a trajectory can thus be compared with each other, and 3-D cluster graphs are generated in which each data point represents a comparison of two trajectory frames plotted in time (x and y axes) and rms deviation (z axis). Each data point is color-coded according to increment Å-rms deviation and is thus representative of how a given trajectory frame compares with another. From the cluster graphs, different points were selected in the low- and high-rms regions, and heme electrostatic potential maps were obtained for these pairs of substates. These maps were generated using the Grasp software package (Nicholls et al., 1991), which includes a Poisson-Boltzmann (PB) solver, essentially a graphical version of the finite-difference solutions to the PB equation, which are implemented in the Delphi software package

(Jayaram et al., 1989; Nicholls and Honig, 1991). Briefly, the spatial variation of the potential Φ at position $\mathbf{r}$ is related to the charge distribution ρ and the position-dependent dielectric permittivity ϵ as follows:

$$\nabla\epsilon(\mathbf{r})\nabla\Phi(\mathbf{r}) = -4\pi\rho(\mathbf{r})/kT \quad (6)$$

If mobile ions are present in the system, the Poisson equation can be combined with the Boltzmann expression for ion concentration, yielding

$$\nabla\epsilon(\mathbf{r})\nabla\Phi(\mathbf{r}) - \epsilon\kappa^2\Phi(\mathbf{r}) = -4\pi\rho^{\mathrm{f}}(\mathbf{r})/kT \quad (7)$$

where the linearized form of the Poisson-Boltzmann equation is sufficient for most protein applications. The term κ^2 is equal to $1/\lambda^2$ or $8\pi q^2 I/ekT$, where λ is the Debye length, I is the ionic strength of the solution, and ρ^{f} is the fixed charge density. Φ, ϵ, κ, and ρ are all functions of the vector $\mathbf{r}$. The second term in Eq. 7 describes the salt effect. Because water molecules are more polarized by an electric field than is the protein, the use of two dielectric constants allows for consideration of the solvation effect experienced by polar molecules in an aqueous solution. The derivative of $\epsilon(\mathbf{r})$ in Eqs. 6 and 7 is nonzero only when $\epsilon(\mathbf{r})$ varies, representing the "dielectric discontinuity" region between the low dielectric solute (protein) and the high dielectric solvent or "molecular surface." The Grasp PB solver uses two 33 cubed grids, one nested within the other. Electrostatic parameters were set as follows: $\epsilon_{\mathrm{inner}} = 2.0$; $\epsilon_{\mathrm{outer}} = 79.0$; water probe radius: 1.4 Å; ionic radius = 2.0 Å; salt concentration: 0.010 M. All calculations were performed using the PARSE (parameters for solvation energy) charge set (Sitkoff et al., 1994), with titratable residues corresponding to their neutral pH charge.

RESULTS

SHB in HHZnc

Fig. 2 shows the Stark effect pattern observed for HHZn*c*. In a previous study (Köhler et al., 1997), we showed that HHZn*c* exists in the neutral pH range in two spectrally distinct forms, which we labeled the "red" conformation (lower energy) and the "blue" conformation (higher energy).

The origins of the lowest frequency electronic transitions of the "red" and "blue" conformations are observed at 17,007 cm^{-1} and 17,114 cm^{-1}, respectively. As narrow holes (i.e., holes with a width of 1 GHz or less) cannot be burned in the peaks observed in the 17,200–17,400 cm^{-1} range, they have to be assigned to vibronic or higher electronic transitions. The lifetime of the excited state of such transitions is significantly decreased in comparison to the lifetime of the lowest energy electronic transition, so the homogeneous line width and, hence, the hole width are strongly increased. In our example, the hole widths in the blue wing of the Q(0,0) range appear to be so large that they cannot be determined within the 30-GHz scan range of the laser.

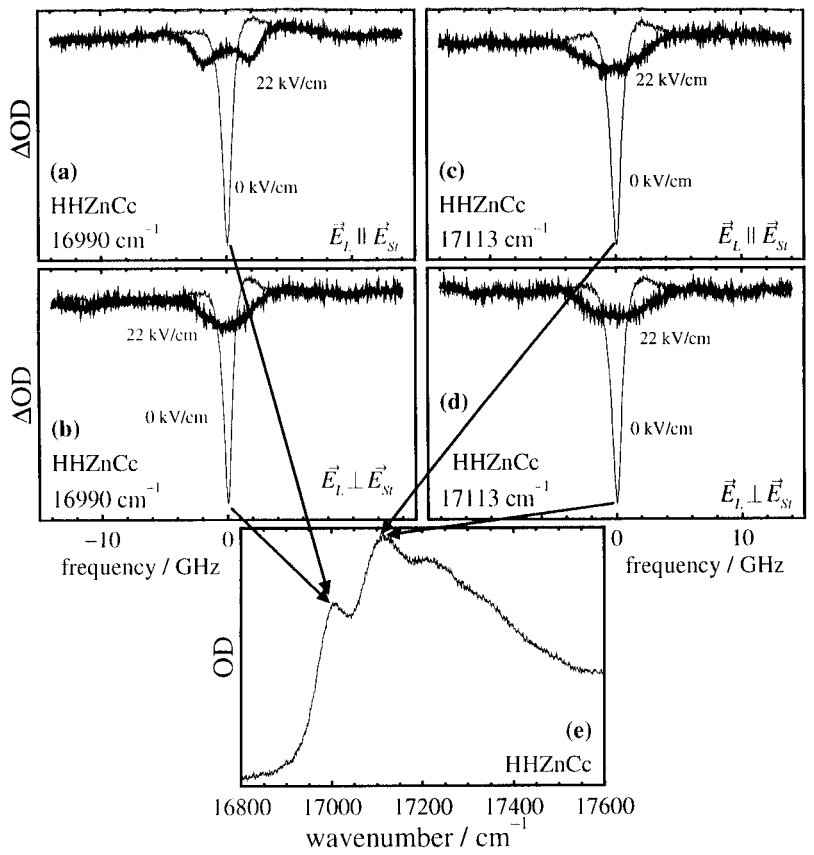

FIGURE 2 Absorption spectrum and hole burning Stark effect of HHZn*c*. (*a* and *b*) Stark effect at ν = 16,990 cm^{-1}. (*a*) $\mathbf{E}_{\mathrm{L}} \parallel \mathbf{E}_{\mathrm{St}}$. (*b*) $\mathbf{E}_{\mathrm{L}} \perp \mathbf{E}_{\mathrm{St}}$. (*c* and *d*) Stark effect at ν = 17,113 cm^{-1}. (*c*) $\mathbf{E}_{\mathrm{L}} \parallel \mathbf{E}_{\mathrm{St}}$. (*d*) $\mathbf{E}_{\mathrm{L}} \perp \mathbf{E}_{\mathrm{St}}$. (*e*) Absorption spectrum of the Q(0,0)-range. The arrows mark the burning frequencies.

The behaviors of the two conformations in an electric field differ. In the "red" conformation, we observe a clear splitting of the hole under parallel polarization. It points to a dipole moment difference with an angle to the transition dipole moment smaller than 55°. However, in the "blue" conformation, one recognizes a flattening of the hole under perpendicular polarization. The flattening can be interpreted as a splitting that is too small to be resolved. According to a fit, the angle between the dipole moment difference and the transition dipole moment is larger than 55° in the "blue" conformation.

SHB in YZn*c*

Fig. 3 shows the hole burning results in YZn*c*. A comparison of the absorption spectra of YZn*c* and HHZn*c* shows characteristic differences. It seems that the "red" band is missing in YZn*c*. Instead, the lowest energy band in YZn*c* is almost at the same frequency position as the "blue" band in HHZn*c*. From this, one might already guess that there is only one conformation and one Stark pattern in the entire Q(0,0) range of YZn*c*. Because the lowest energy transition of YZn*c* has almost the same frequency as the "blue" conformation of HHZn*c*, it is reasonable to assume that the pocket structure and, hence, the Stark pattern of YZn*c* are similar to those of the "blue" HHZn*c* conformation. This is exactly what we observe; we performed hole burning Stark effect experiments within the whole frequency range of YZn*c* that allows narrow band hole burning. The Stark pattern was the same at all frequencies; we observe a stronger broadening under perpendicular polarization than under parallel polarization. This points to an unresolved splitting under perpendicular polarization, very similar to that in the "blue" conformation of HHZn*c*. We stress that narrow hole burning in the pronounced peak around 17,250 cm^{-1} (Fig. 3) is not possible. Hence this peak does not correspond to another conformational origin. Instead, it must be related to a higher electronic or vibrational transition.

Electrostatic sampling of heme potentials

Fig. 4 shows representative clustering graphs obtained for two different MDS trajectories. The regions of low rms are near the diagonal, and these data points represent topographical substates that are relatively close in the trajectory. We note that the rms values distribute differently in HHZn*c* when compared to YZn*c*. The former sample consists of three rms regions (white = 0 < rms < 1; blue = 1 < rms < 2; red = 2 < rms < 3) as opposed to two (white and blue) for the latter. Fig. 5 shows the superimposed backbones of two HHZn*c* trajectory frames taken from the high-rms region of the cluster graph. Similar patterns were obtained for all six trajectories recorded for both cytochromes. Forty-one sets were then randomly selected for graphical modeling of the heme electrostatic potential surfaces. Fig. 6 displays the potential surfaces generated for four sets of two different HHZn*c* substates (*left-hand side and right-hand side*) selected in the region of high rms of the cluster graph; these are representative of two different topographical substates. Fig. 7 presents similar heme electrostatic potential maps for YZn*c*. In all such Grasp renderings, the heme potential surfaces of HHZn*c* high-rms difference pairs were observed to be "electrostatically" different. Tables 2 and 3 list the potentials and electric fields calculated at the pyrrole nitrogens for pairs of substates selected from the cluster analysis for both HHZn*c* and YZn*c*. $\mathbf{E}_x$, $\mathbf{E}_y$, and $\mathbf{E}_z$ are the respective electric field components calculated at the pyrrole nitrogens in the *x*, *y*, *z* directions. All MDS frames were oriented with the porphyrin in the *x*-*y* plane, and with the *z* axis normal to the heme plane, before potentials and field vectors were calculated. In the context of our work, the $\mathbf{E}_x$ and $\mathbf{E}_y$ values presented for the NA, NC nitrogens (bold type) are espe-

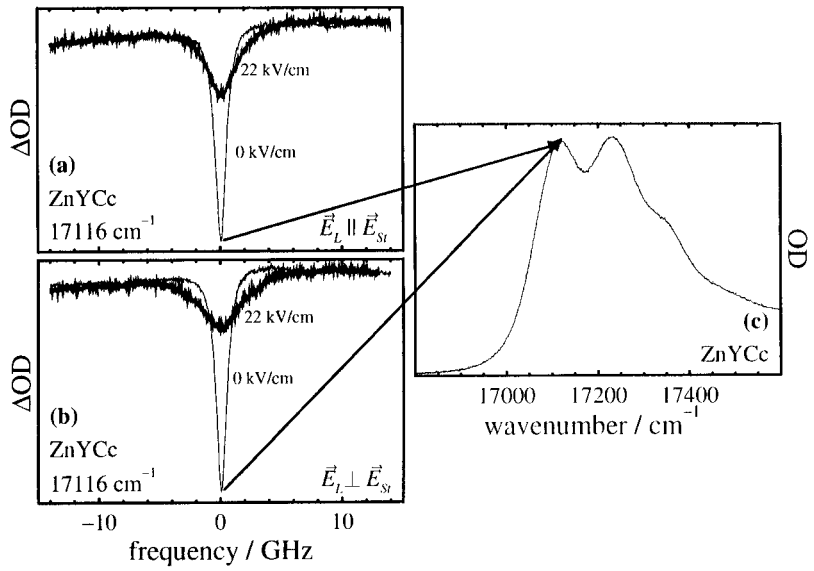

FIGURE 3 Absorption spectrum and hole burning Stark effect of YZn*c*. (*a* and *b*) Stark effect at ν = 17,116 cm^{-1}. (*a*) $\mathbf{E}_L \parallel \mathbf{E}_{St}$. (*b*) $\mathbf{E}_L \perp \mathbf{E}_{St}$. (*c*) Absorption spectrum of the Q(0,0)-range. The arrows mark the burning frequency.

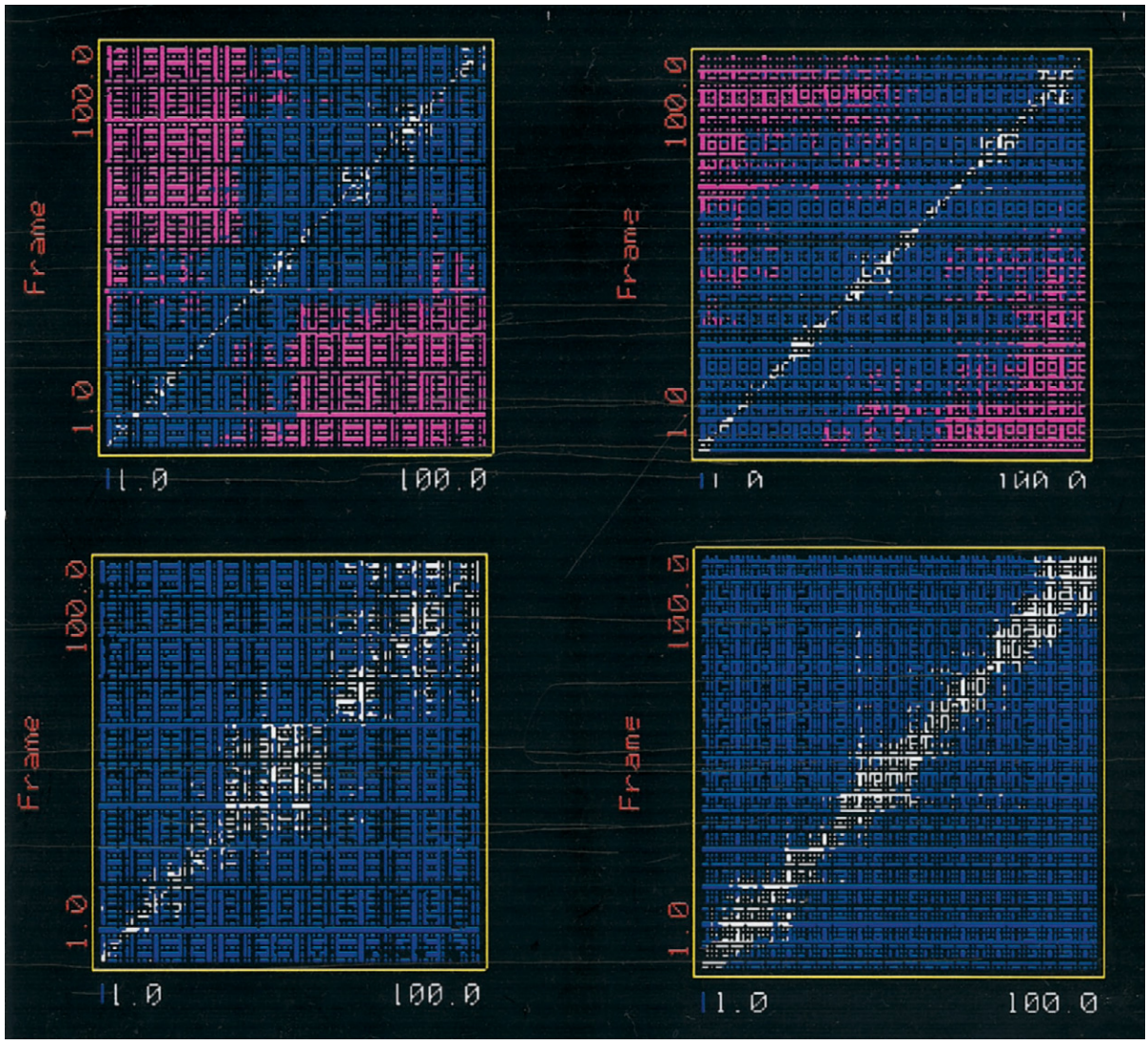

FIGURE 4 Representative cluster graphs comparing HHZn*c* (*top*) and YZn*c* (*bottom*) MDS trajectories. The *x* and *y* axes represent the number of frames in the trajectory, selected with a step of 5; thus 100 frames = 500 ps. The *z* axis represents the rms value. The data points are color-coded according to the rms value of two compared trajectory frames: white = $0 \leq$ rms < 1; blue = $1 <$ rms < 2; red = $2 <$ rms < 3. Comparing a given frame with itself yields a rms of 0. The graph is symmetrical about the diagonal.

cially relevant because these atoms represent the axis of the electronic transition dipole (cf. Fig. 1). The tables are organized as follows: in Table 2, Hi-rms pair 1 was extracted from the high-rms (red) region of the cluster graph (Fig. 4); SSa and SSb thus represent two dissimilar substates (with high rms difference). Line 1 thus horizontally reads for pyrrole nitrogen NA the comparative potential and electric field component values for both substates (SSa and SSb). Table 3 has the same format, except that all values are for similar substates, because cluster analysis revealed no significantly different topographical groupings for YZn*c*.

DISCUSSION

The SHB results obtained for the two cytochromes are clearly indicative of different spectral populations: in HHZn*c*, we assign the two populations revealed by different SHB patterns to two distinct Q_x components, namely Q_{xI} (17,007 cm^{-1}) and Q_{xII} (17,114 cm^{-1}). In this view, the respective Q_{yI} and Q_{yII} are buried in the inhomogeneous spectral envelope. In YZn*c*, there is only one spectral population, with Q_x observed at 17,116 cm^{-1}. Such distinct spectral conformations have recently been observed in the horseradish peroxidase system, using a combination of pressure-tuning and Stark effect SHB techniques (Balog et al., 1997), and we believe that we are also observing different protein substates in HHZn*c*, characterized by different pocket fields.

The MDS cluster graphs (Fig. 4) also clearly show that HHZn*c* and YZn*c* do not explore conformational space in the same way, with the former exploring conformational space with more flexibility (maximum backbone rms for the

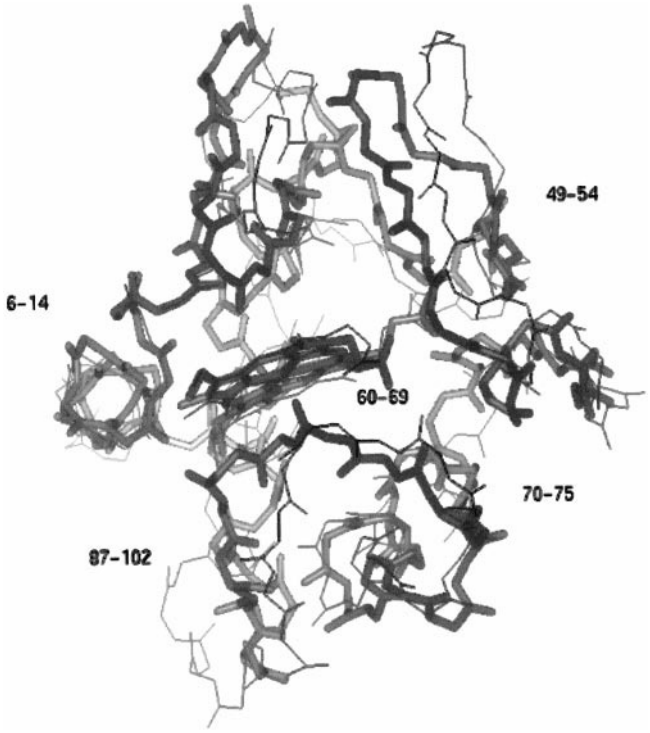

FIGURE 5 Rendering of superposed backbones for two HHZn*c* substates (*thick and thin lines*, respectively) extracted from the high rms region of a cluster graph. The labeling refers to the three major helices of cytochrome *c*, involving residues 6–14, 60–69, and 87–102, and the three minor helical segments involving residues 49–54 and 70–75 (Bushnell et al., 1990).

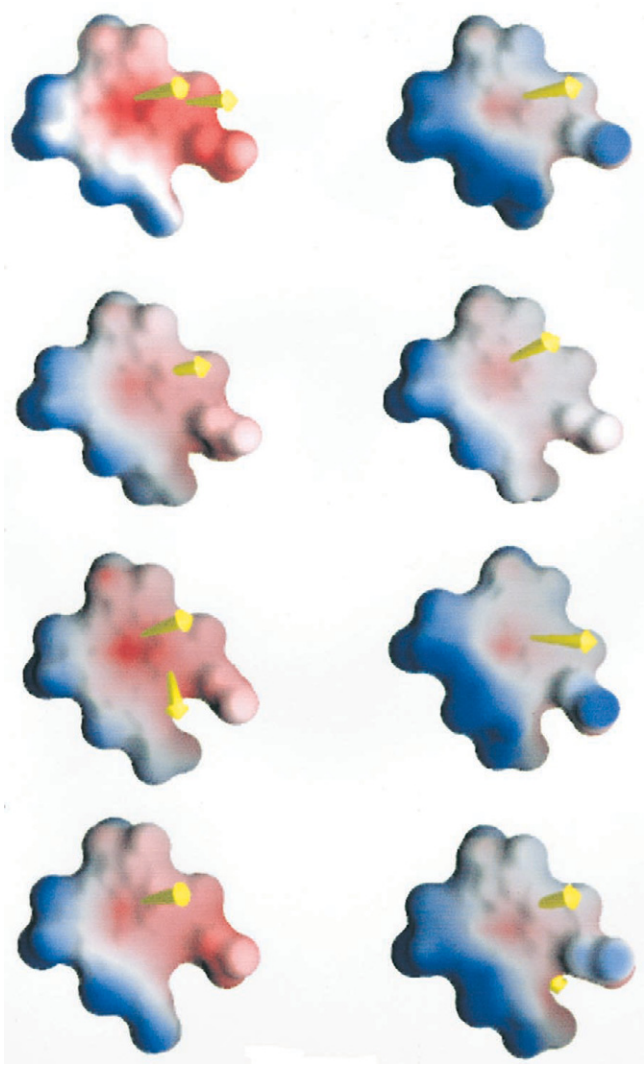

FIGURE 6 *Grasp* visualization of HHZn*c* heme electrostatic potentials showing the difference in calculated potentials at the heme of substates selected in different rms-substate groupings. The heme potential surfaces are color-coded: red = more negative, −380 mV; blue = more positive, −35 mV. The left-hand-side and right-hand-side figures represent hemes from substates with significant backbone rms difference. The yellow arrows are the (constant length) resultants of the electric field vectors calculated at both NA and NC pyrrole nitrogens. Note that the full rendering of the heme potential surfaces sometimes makes it impossible to clearly see that they originate at these atoms. When only one is seen, the direction of the other resultant is on the other side of the potential map.

HHZn*c* trajectories: 3.9 Å versus 2.2 Å for YZn*c*). On the basis of this rms distinction, the HHZn*c* trajectory topographical frames can be grouped into two major substate populations. The first question to be addressed in this context is how representative of different protein conformations these rms regions are, especially with values that are not indicative of extreme structural rearrangement. During the trajectories, as expected from such rms values, helical structure is never lost, whether in the three major helices or in the two helical segments. Rather, the helical structures are displaced from each other when two high-rms substates are compared to each other or to the starting x-ray structure. This is shown in Fig. 5, which displays the superimposed backbones of two HHZn*c* trajectory frames extracted from the high-rms region of the cluster graph. It is as if one substate is more expanded when compared to the other, for example, as seen in the 49–54 helix region and in the 87–102 helical region as well. One immediate consequence of such a displacement—especially of the 87–102 helix—would be to reorganize the H-bonding network on the Met-ligand side of the heme, which has already been shown in site mutagenesis studies to be of crucial importance in the control of electrostatic interactions in the heme pocket and charge interactions at the heme (Hildebrandt et al., 1993).

The Grasp renderings shown in Figs. 6 (HHZn*c*) and 7 (YZn*c*) lead us to propose the existence of clearly distinguishable "electrostatic substates" rather than purely structural ones. We stress that not all structural substates are necessarily characterized by specific distinguishable electrostatic features. On the other hand, as our calculations show, rather small structural changes may lead in some cases to remarkably different fields at the heme site. The heme potential maps generated for HHZn*c* reflect a first such substate (Fig. 6, *left-hand side*), whose trajectory frames all show a region distinctly more negative (*red*) than that calculated for the second substate (Fig. 6, *right-hand side*). Inspection of the YZn*c* potential surfaces (Fig. 7) shows no such distinguishable substates, but these surfaces

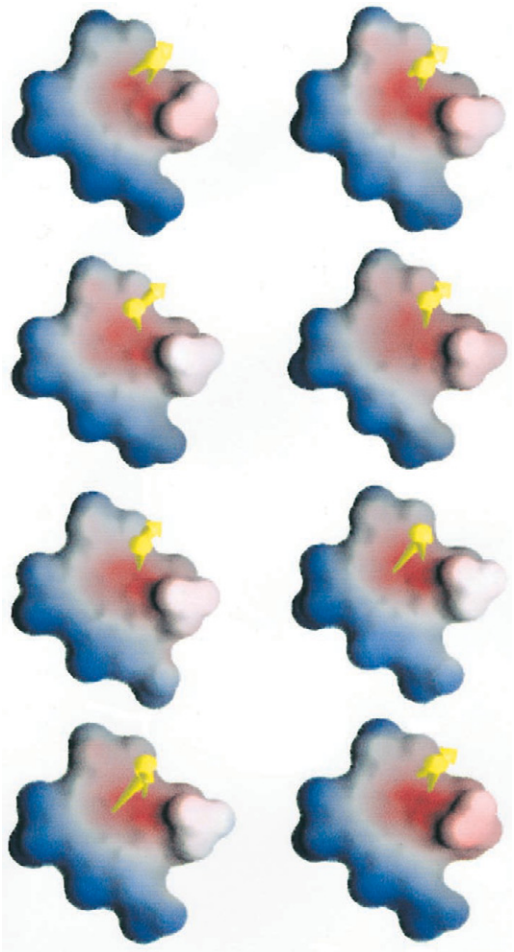

FIGURE 7 *Grasp* visualization of YZn*c* heme electrostatic potentials, showing the difference in calculated potentials at the heme of substates selected in the single rms-substate grouping. The heme potential surfaces are color-coded: red = more negative, −580 mV; blue = more positive, −35 mV. The left-hand-side and right-hand-side figures represent hemes from frames with insignificant backbone rms difference. The yellow arrows are the resultant of the electric field vectors calculated at NA and NC for all hemes.

are representative of rather uniform potentials at the heme. Of notable interest here is that the $Q_{0,0}$ band in which we perform the SHB is assigned to a a_{1u}, $a_{2u} \rightarrow e_g$ transition, the transition dipole of which is aligned along the NA-NC axis in the four-orbital model (Gouterman, 1978). The resultant of the electric field *x*, *y*, and *z* components calculated at these atoms (*yellow arrows*) is seen to be more heterogeneous in the left-hand HHZn*c* than in the case of the right-hand substate, where they have almost the same direction, as is the case for all YZn*c* frames (Fig. 7). This is confirmed by the more exact calculations performed with Delphi. Inspection of the in-plane $\mathbf{E}_x$ and $\mathbf{E}_y$ components (Table 2) obtained for the HHZn*c* high-rms pairs of substates shows substantially different field strengths along the electronic transition axis (bold type), with one exception, pair 1, which displays similar $\mathbf{E}_x$ values ($-7.9kT$/eÅ and $-6.3kT$/eÅ, respectively). This does not invalidate the point that different "electrostatic substates" should generate different fields at the heme; this could be due to coincidence. All other $\mathbf{E}_x$ and $\mathbf{E}_y$ are consistent with significant field heterogeneity along the transition dipole axis between different substates. Examination of the $\mathbf{E}_x$ and $\mathbf{E}_y$ values calculated for YZn*c* (Table 3) shows the opposite trend: the electric field is remarkably uniform along the transition axis.

The question immediately arises: what factor(s) could possibly account for the spectrally and electrostatically distinguishable substates of HHZn*c*? We analyzed the variation in heme geometry in the trajectories to detect possible significant heme distortions in time, focusing on geometries indicative of heme planarity distortions, such as the distance between C3B and SG (cf. Fig. 1 and Fig. 8, *bottom*), previously shown to be sensitive to pyrrole twisting (Laberge et al., 1998) and the ZN-NC-C1C-C2C and ZN-NB-C4B-C3B dihedrals (not shown), as well as other markers of out-of-plane and in-plane distortions known to be typical of the cytochrome *c* heme distortion (Jentzen et al., 1997). All such plots showed that the specific cytochrome *c* heme distortion is maintained throughout the trajectories. This is not surprising, as it is in full agreement with recent molecular mechanics studies showing that the nonplanarity of the heme in cytochromes is highly conserved (Jentzen et al., 1998). We also monitored the heme propionate flexibility during the trajectories (Fig. 8, *top*) to see if it would be possible to identify two types of propionate motion in the HHZn*c* trajectories that could account for the two "electrostatic substates." Clearly, the propionates sample conformational space rather uniformly, not only in the HHZn*c* trajectories but in the YZn*c* ones as well.

The charge reorganization at the heme of HHZn*c* can thus be attributed to the fluctuating protein matrix fields during conformational space sampling. The existence of such electrostatic conformers has been proposed from ps-MDS studies of tuna cytochrome *c*, which predicted the occurrence of transient high-potential sites—associated with side-chain reorientations—that could facilitate the association of charged substrates and play a role in catalysis (Wendoloski and Matthew, 1989). In photosynthetic systems, H-bonding interactions have been shown to affect the absorption spectrum of chlorophyll *a* (Eccles and Honig, 1983). It has also been proposed that the protein forms an electric field around the chromophore, capable of interacting and perturbing the electronic energy levels by polarizing the chromophore. MO calculations have shown that a single charge placed close to the chlorophyll ring could strongly affect the orbital energy levels, and thus the absorption spectrum and NMR shifts have been predicted for the Q_y transition of chlorophyll *a*. It thus does not seem unreasonable to conclude that in HHZn*c* and YZn*c*, the respective pocket fields around the heme chromophore are subject to different protein-induced electrostatic perturbations that interact with the electronic levels of the heme, thus accounting for the different SHB profiles observed in the two cytochromes. This view also implies that the dipole moment difference that we observe

TABLE 2 Electrostatic potentials and fields calculated at the heme pyrrole nitrogens for superposed HHZn*c* substate pairs (SSa and SSb) with high rms values sampled during a 1-ns MDS trajectory

Hi-rms pair no.	Pyrrole N-atom	Potential (*kT*/e)		E_x (*kT*/eÅ)		E_y (*kT*/eÅ)		E_z (*kT*/eÅ)	
		SSa	SSb	SSa	SSb	SSa	SSb	SSa	SSb
1	**NA**	**−324.3**	**−259.1**	**−7.9**	**−6.3**	**−3.47**	**−0.9**	**1.8**	**9.1**
	NB	−268.2	−206.4	−22.2	−26.9	−16.8	−19.4	−19.6	−18.5
	NC	**−212.5**	**−143.2**	**−39.2**	**−41.4**	**4.8**	**3.7**	**−18.5**	**−15.0**
	ND	−264.7	−198.3	−28.9	−29.7	25.9	25.3	−7.9	5.3
2	**NA**	**−345.6**	**−274.2**	**−8.4**	**1.3**	**−9.9**	**−2.6**	**1.1**	**9.7**
	NB	−281.3	−243.3	−22.7	−16.2	−18.4	−11.0	−13.4	−14.2
	NC	**−229.6**	**−177.2**	**−43.4**	**−41.3**	**1.6**	**11.8**	**−14.7**	**−20.1**
	ND	−292.3	−227.8	−35.2	−30.8	16.5	18.2	−3.8	−5.4
3	**NA**	**−317.3**	**−240.6**	**−8.9**	**−4.5**	**−5.6**	**−11.1**	**−4.3**	**0.3**
	NB	−244.9	−188.5	−23.6	−15.1	−16.9	−16.6	−19.7	−15.4
	NC	**−189.6**	**−142.9**	**−45.2**	**−35.2**	**1.5**	**6.7**	**−31.8**	**−19.9**
	ND	−258.1	−187.0	−34.1	−33.2	20.8	22.0	−9.2	2.3
4	**NA**	**−312.0**	**−244.9**	**−8.9**	**−7.7**	**−5.4**	**0.2**	**0.1**	**6.9**
	NB	−255.8	−196.6	−23.2	−25.5	−17.4	−13.1	−15.2	−6.1
	NC	**−194.0**	**−141.9**	**−46.9**	**−35.5**	**3.6**	**2.9**	**−20.9**	**−5.9**
	ND	−253.0	−180.4	−32.7	−28.8	18.9	25.7	−8.6	−15.2

Note that $kT/eÅ = 2.59 \times 10^6$ V/cm at 300 K.

in the Stark experiments (splitting in Fig. 2 *a*) is not correlated with the charge at the propionics because this charge is not changed as the protein moves within its conformational space. However, we must bear in mind that at this point we cannot quantitatively correlate the observed Stark effects with the calculated potentials. In the case of biological chromophores, structure-spectra correlations are highly complex, one of the major problems being to account for solvent effects on the electronic transitions because the changes in solute-solvent interaction upon electronic excitation have to be evaluated. This is a very challenging task, as such treatment must include dispersion, polarization, charge-charge interactions, and the effect of solvent-induced dipoles to yield reasonably meaningful results (Luzhkov and Warshel, 1991).

SUMMARIZING CONCLUSIONS

Stark effect hole burning experiments clearly show that cytochrome *c*-type proteins from two different sources (horse heart and yeast) exist in different substructures. In HHZn*c* two structural states with remarkably different electrostatic properties could be identified. In YZn*c* there is just one state that seems to be very similar to one of the two states in HHZn*c*. The results from Stark effect spectroscopy are strongly supported by molecular dynamics and electrostatic calculations: the fluctuations of the conformation space sampled by the proteins are significantly larger for HHZn*c* than for YZn*c*. The larger variations in structure correlate with clearly distinguishable features of the electric field at the heme site.

TABLE 3 Electrostatic potentials and fields calculated at the heme pyrrole nitrogens for superposed YZn*c* substate pairs (SSa and SSb) sampled during a 1-ns MDS trajectory

Lo-rms pair no.	Pyrrole N-atom	Potential (*kT*/e)		E_x (*kT*/eÅ)		E_y (*kT*/eÅ)		E_z (*kT*/eÅ)	
		SSa	SSb	SSa	SSb	SSa	SSb	SSa	SSb
1	**NA**	**−355.9**	**−354.9**	**−3.3**	**−4.4**	**16.2**	**14.8**	**−46.0**	**−46.6**
	NB	−327.0	−330.6	−25.5	−22.4	−12.8	−13.2	−12.4	−16.1
	NC	**−235.4**	**−235.1**	**−50.2**	**−47.1**	**24.5**	**25.1**	**−20.4**	**−20.5**
	ND	−242.3	−245.1	−30.5	−30.4	45.6	42.1	−30.6	−32.0
2	**NA**	**−312.0**	**−342.9**	**−2.9**	**−0.8**	**15.6**	**14.1**	**−45.7**	**−37.4**
	NB	−343.8	−341.6	−18.9	−17.2	−12.2	−10.4	−14.5	−10.5
	NC	**−249.9**	**−257.0**	**−44.3**	**−44.5**	**23.8**	**26.2**	**−18.0**	**−15.0**
	ND	−248.7	−253.3	−26.6	−23.5	40.8	41.7	−30.9	−30.8
3	**NA**	**−349.7**	**−341.5**	**−1.6**	**−4.6**	**20.9**	**17.9**	**−40.0**	**−41.3**
	NB	−354.5	−339.3	−21.5	−16.5	−6.4	−10.1	−10.3	−10.8
	NC	**−243.6**	**−242.1**	**−49.3**	**−44.5**	**25.2**	**29.7**	**−15.6**	**−14.2**
	ND	−247.0	−252.4	−26.5	−29.5	44.0	42.8	−28.2	−27.1
4	**NA**	**−341.8**	**−342.5**	**0.5**	**2.1**	**16.9**	**24.1**	**−42.9**	**−40.9**
	NB	−335.5	−353.8	−17.8	−18.8	−11.1	−6.5	−6.4	−13.3
	NC	**−245.3**	**−251.6**	**−44.1**	**−44.7**	**26.5**	**30.2**	**−16.1**	**−13.3**
	ND	−244.3	−247.9	−24.3	−24.0	43.4	44.0	−30.5	−24.8

Note that $kT/eÅ = 2.59 \times 10^6$ V/cm at 300 K.

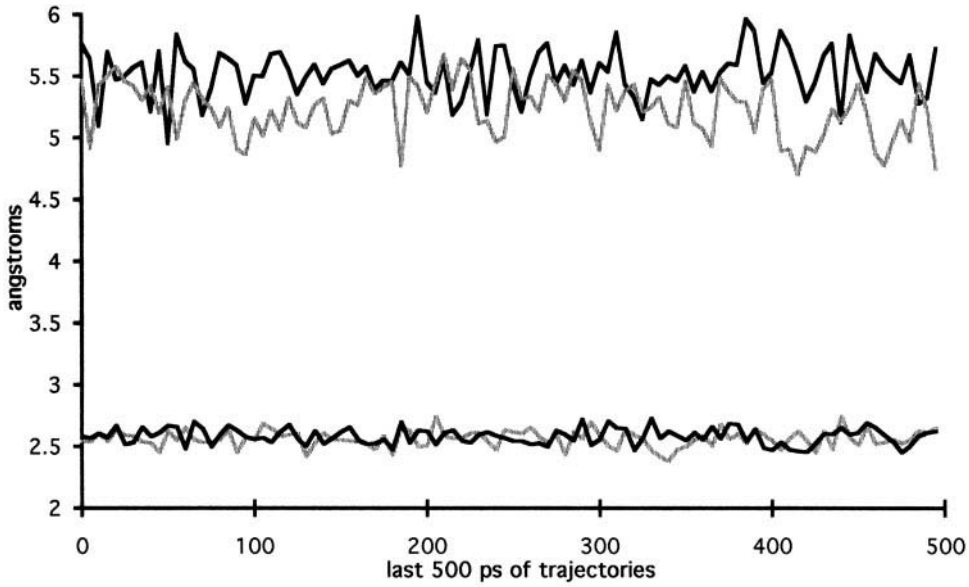

FIGURE 8 O1D-CHA (*top*) and SG-C3B (*bottom*) distances plotted as a function of time for the last 500 ps of a 1-ns MDS run for HHZn*c* (*black line*) and YZn*c* (*gray line*). Compare Fig. 1 for atom nomenclature.

There is one further point that should be stressed: MDS is performed at ambient temperatures, whereas the Stark experiments were carried out at liquid He temperature. However, conformational relaxation slows rapidly down as the temperature is decreased. Hence there is good reason to assume that conformational trapping may already occur at sufficiently high temperatures, so that the conformations probed in the low-temperature Stark experiments do correspond with the structures calculated with MDS.

This research was supported by National Institutes of Health (National Institutes of Health) grant RO1-GM55004 and by National Science Foundation US-Germany International Cooperative Research grant 9513315. We also gratefully acknowledge the kind assistance provided by Dr. G. Keserü from the Department of Chemical Engineering at the Technical University of Budapest (BME), for generous use of his CPU time and Delphi software when our own computational facilities were down. JF gratefully acknowledges the support by the Fonds der Chemischen Industrie. We also gratefully acknowledge critical revision of the manuscript and valuable suggestions by J. Fidy, SOTE Institute of Biophysics, Budapest.

REFERENCES

Adar, F. 1978. Electronic absorption spectra of hemes and heme proteins. *In* The Porphyrins, Vol. III. D. Dolphin, editor. Academic Press, New York. 167–209.

Avbelj, F., and J. Moult. 1995. Role of electrostatic screening in determining protein main chain conformational preferences. *Biochemistry.* 34: 755–764.

Balog, E., K. Kis-Petik, J. Fidy, M. Köhler, and J. Friedrich. 1997. Interpretation of multiple $Q_{0,0}$ bands in the absorption spectrum of Mg-mesoporphyrin embedded in horseradish peroxidase. *Biophys. J.* 73:397–405.

Bernstein, F. C., T. F. Koetzle, G. J. B. Williams, E. F. Meyer, Jr., M. D. Brice, J. R. Rodgers, O. Kennard, T. Shimanouchi, and M. Tasumi. 1977. The Protein Data Bank: a computer-based archival file for macromolecular structures. *Eur. J. Biochem.* 80:319–324.

Burns, P. D., and G. N. La Mar. 1981. Characterization of conformational heterogeneity in the heme pocket of ferricytochrome *c* using high field proton nuclear magnetic resonance spectroscopy. *J. Biol. Chem.* 256: 4934–4939.

Bushnell, G. W., G. V. Louie, and G. D. Brayer. 1990. High-resolution three-dimensional structure of horse heart cytochrome *c*. *J. Mol. Biol.* 214:585–595.

Campbell, B. F., M. R. Chance, and J. M. Friedman. 1987. Linkage of functional and structural heterogeneity in proteins: dynamic hole burning in carboxymyoglobin. *Science.* 238:373–376.

Davies, A. M., J. G. Guillemette, M. Smith, C. Greenwood, A. G. P. Thurgood, A. G. Mauk, and G. R. Moore. 1993. Redesign of the interior hydrophilic region of mitochondrial cytochrome *c* by site-directed mutagenesis. *Biochemistry.* 32:5431–5435.

Dickerson, R. E., and R. Timkovich. 1975. Cytochrome *c*. *In* The Enzymes. Academic Press, New York. 398–547.

Ding, H. Q., N. Karasawa, and W. A. Goddard. 1992. Atomic level simulations on a million particles: the cell multipole method for Coulomb and London nonbond interactions. *J. Chem. Phys.* 97:4309–4320.

Eccles, J., and B. Honig. 1983. Charged amino acids as spectroscopic determinants for chlorophyll in vivo. *Proc. Natl. Acad. Sci. USA.* 80: 4959–4962.

Frauenfelder, H., and P. G. Wolynes. 1994. Biomolecules: where the physics of complexity and simplicity meets. *Physics Today.* 47:58–64.

Furenlid, L. R., M. W. Renner, and J. Fajer. 1990. EXAFS studies of nickel(II) and nickel(I) factor 430 M. Conformational flexibility of the F430 skeleton. *J. Am. Chem. Soc.* 112:8987–8989.

Gafert, J., J. Friedrich, and F. Parak. 1995. Stark effect experiments on photochemical holes in chromoproteins: protoporphyrin IX substituted myoglobin. *Proc. Natl. Acad. Sci. USA.* 92:2116–2120.

Gottfried, D. S., M. A. Steffen, and S. G. Boxer. 1991. Large protein-induced dipoles for a symmetric carotenoid in a photosynthetic antenna complex. *Science.* 251:662–665.

Gouterman, M. 1978. Optical spectra and electronic structure of porphyrins and related rings. *In* The Porphyrins. Academic Press, New York. 1–156.

Grewer, G., and M. Lösche, 1991. Concentration dependence of the electrooptical spectra from two dimensional aggregated chromophore systems. *Makromol. Chem. Symp.* 46:79–87.

Gunner, M. R., and B. Honig. 1991. Electrostatic control of midpoint potentials in the cytochrome subunit of the *Rhodopseudomonas viridis* reaction center. *Proc. Natl. Acad. Sci. USA.* 88:9151–9155.

Harvey, S. C. 1989. Treatment of electrostatic effects in macromolecular modeling. *Proteins Struct. Funct. Genet.* 5:78–92.

Hildebrandt, P., F. Vanhecke, G. Heibel, and G. Mauk. 1993. Structural changes in cytochrome *c* upon hydrogen-deuterium exchange. *Biochemistry.* 32:14158–14164.

Hobbs, J. D., and J. R. Shelnutt. 1995. Conserved nonplanar heme distortions in cytochromes *c*. *J. Protein Chem.* 14:19–25.

Jayaram, B., K. A. Sharp, and B. Honig. 1989. The electrostatic potential of B-DNA. *Biopolymers.* 28:975–993.

Jentzen, W., J.-G. Ma, and J. A. Shelnutt. 1998. Conservation of the conformation of the porphyrin macrocycle in hemeproteins. *Biophys. J.* 74:753–763.

Jentzen, W., W.-Z. Song, and J. A. Shelnutt. 1997. Structural charaterization of synthetic and protein-bound porphyrins in terms of the lowest-frequency normal coordinates of the macrocycle. *J. Phys. Chem. B.* 101:1684–1699.

Kohler, B. E., R. I. Personov, and J. C. Woehl. 1994. Electric field effects in molecular systems studied via persistent hole burning. *In* Laser Techniques in Chemistry. Th. Rizzo and A. B. Myers, editors. chap. 8. Wiley, New York. 283–323.

Köhler, M., J. Friedrich, and J. Fidy. 1998. Proteins in electric fields and pressure fields: basic aspects. *Biochim. Biophys. Acta.* 1386:255–288.

Köhler, M., J. Gafert, J. Friedrich, J. M. Vanderkooi, and M. Laberge. 1996. Stark-effect experiments in cytochrome *c*-type proteins: structural hierarchies. *Biophys. J.* 71:77–85.

Köhler, M., M. Laberge, J. Friedrich, and J. M. Vanderkooi. 1997. Influence of pH on the pocket field of c-type proteins as monitored by hole burning spectroscopy. *Chem. Phys.* 224:327–335.

Laberge, M. 1998. Intrinsic protein electric fields: basic non-covalent interactions and relationship to protein-induced Stark effects. *Biochim. Biophys. Acta.* 1386:305–330.

Laberge, M., J. M. Vanderkooi, and K. A. Sharp, 1996. Effect of a protein field on the CO stretch frequency. FDPB calculations on carbonmonoxy cytochrome *c*. *J. Phys. Chem.* 100:10793–10801.

Laberge, M., A. Vreugdenhil, J. M. Vanderkooi, and I. S. Butler. 1998. Microperoxidase-11: molecular dynamics and Q-band excited resonance Raman of the oxidized, reduced and carbonyl forms. *J. Biomol. Struct. Dyn.* 15:1039–1050.

Lamotte-Brasseur, J., G. Dive, D. Dehareng, and J. M. Ghuysen. 1990. Electrostatic potential maps at the quantum chemistry level of the active site of the serine peptidases, alpha-chymotrypsin and subtilisin. *J. Theor. Biol.* 145:183–198.

Langen, R., G. D. Brayer, A. M. Berghuis, G. McLendon, F. Sherman, and A. Warshel. 1992. Effect of the $Asn^{52}\rightarrow$Ile mutation on the redox potential of yeast cytochrome *c*. Theory and experiment. *J. Mol. Biol.* 224:589–600.

Loew, G. H. 1983. Theoretical investigations of iron porphyrins. *In* Iron Porphyrins. Addison-Wesley, London. 1–87.

Louie, G. V., and G. D. Brayer. 1990. High-resolution refinement of yeast iso-1-cytochrome *c* and comparison with other eukaryotic cytochromes *c*. *J. Mol. Biol.* 214:527–555.

Luzhkov, V., and A. Warshel. 1991. Microscopic calculation of solvent effects on absorption spectra of conjugated molecules. *J. Am. Chem. Soc.* 113:4491–4499.

Maier, M. 1986. Persistent spectral holes in external fields. *Appl. Phys. B.* 41:73–90.

Nicholls, A., and B. Honig. 1991. A rapid finite difference algorithm utilizing successive over-relaxation to solve the Poisson-Boltzman equation. *J. Comp. Chem.* 12:435–445.

Nicholls, A., K. A. Sharp, and B. Honig. 1991. Protein folding and association: insights from the interfacial and thermodynamic properties of hydrocarbons. *Proteins.* 11:281–296.

Northrup, S., T. G. Wensel, C. F. Meares, J. J. Wendoloski, and J. B. Matthew. 1990. Electrostatic field around cytochrome *c*: theory and energy transfer experiment. *Proc. Natl. Acad. Sci. USA.* 87:9503–9507.

Paulsen, M. D., and R. L. Ornstein. 1995. Dramatic differences in the motions of the mouth of open and closed cytochrome P450BM-3 by molecular dynamics simulations. *Proteins.* 21:237–243.

Schätz, P., and M. Maier. 1987. Calculation of electric field effects on persistent spectral holes in amorphous host-guest systems. *J. Chem. Phys.* 87:809–820.

Schmidt, K. E., and M. A. Lee. 1991. Implementing the fast multipole method in three dimensions. *J. Stat. Phys.* 63:1223–1237.

Schmidt, S., and R. Reich. 1972. Über den Einfluss elektrischer Felder auf das Absorptionsspektrum von Farbstoffmolekülen in Lipidschichten. III. Elektrochromie eines Carotenoids (Lutein). *Ber. Bunsenges.* 76: 1202–1208.

Sharp, K., and B. Honig. 1990. Electrostatic interactions in macromolecules: theory and applications. *Annu. Rev. Biophys. Chem.* 19:301–332.

Sitkoff, D., K. A. Sharp, and B. Honig. 1994. Accurate calculation of hydration free energies using macroscopic solvent models. *J. Phys. Chem.* 98:1978–1988.

Sitnitsky, A. E. 1995. Fluctuations of electric field in enzyme active site as an efficient source of reaction activation. *Chem. Phys. Lett.* 240:47–52.

Vanderkooi, J. M., F. Adar, and M. Erecinska. 1976. Metallocytochrome *c*: characterization of electronic absorption and emission spectra of Sn and Zn cytochromes *c*. *Eur. J. Biochem.* 64:381–387.

Warshel, A., and J. Aqvist. 1991. Electrostatic energy and macromolecular function. *Annu. Rev. Biophys. Biophys. Chem.* 20:267–298.

Wendoloski, J., and J. B. Matthew. 1989. Molecular dynamics effects on protein electrostatics. *Proteins.* 5:313–321.

Wright, W. W., M. Laberge, and J. M. Vanderkooi. 1997. Surface of cytochrome *c*: infrared spectroscopy of carboxyl groups. *Biochemistry.* 36:14724–14732.

Zhou, H. X. 1993. Boundary element solution of macromolecular electrostatics: interaction energy between two proteins. *Biophys. J.* 65: 955–963.

Zhou, J. S., and N. M. Kostic. 1993. Comparison of electrostatic interactions and of protein-protein orientations in electron-transfer reactions of plastocyanin with the triplet state of zinc cytochrome and with zinc cytochrome *c* cation radical. *Biochemistry.* 32:4539–4546.